Journal of
Materials Chemistry A

Accepted Manuscript

This article can be cited before page numbers have been issued, to do this please use: Y. Sun, B. Fan, X. Xue, X. Meng, X. Sun, L. Huo and W. Ma, *J. Mater. Chem. A*, 2016, DOI: 10.1039/C6TA05886H.

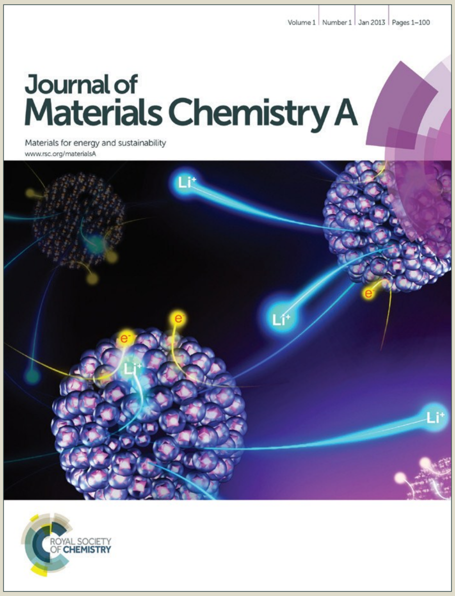

View Article Online
DOI: 10.1039/C6TA05886H

High-Performance Conjugated Terpolymer-Based Organic Bulk Heterojunction Solar Cells

Received 00th January 20xx,
Accepted 00th January 20xx

DOI: 10.1039/x0xx00000x

www.rsc.org/

Bingbing Fan,[a,b] Xiaonan Xue,[a,b] Xiangyi Meng,[c] Xiaobo Sun,* [a,b] Lijun Huo,* [a,b] Wei Ma,*[c] and Yanming Sun* [a,b]

Recently, conjugated terpolymers comprising three components have attracted tremendous attention. However, quite few examples of high-performance terpolymers have been reported. We presented here two novel terpolymers named PtDDA and PtDAA, in which bithiophene (BT) and benzo[1,2-c:4,5-c']dithiophene-4,8-dione (T1) were chosen as the donor and acceptor units, respectively. Thieno[3,2-b]thiophene (TT) and thiazolo[5,4-d]thiazole (TTz) were used as the third component. It is interesting to find that PtDDA terpolymer shows a typical D1-D2-D1-A1 structure while PtDAA shows a D1-A1-D1-A2 structure. Without using additives or post-annealing processes, PtDAA-based solar cells show a high PCE of 8.1%, with an unprecedented fill factor (FF) of 0.74, which is much higher than PtDDA-based devices (PCE = 3.4%, FF = 0.55). The high efficiency of 8.1% is one of the highest values so far for organic solar cells based on conjugated terpolymers. The high performance is mainly ascribed to the efficient carrier transport in PtDAA:PC$_{71}$BM active layer, high crystallinity of PtDAA, and high domain purity. The results suggest that constructing conjugated terpolymers with one donor and two acceptors units is an effective strategy for designing high-performance solar cell materials.

1 Introduction

Solution-processed polymer solar cells (PSCs) have been developed rapidly over the last two decades due to their advantages of light weight, low cost, flexibility and processability for mass productions.[1-6] Nowadays, power conversion efficiencies (PCEs) exceeding 11% have been reported for bulk heterojunction (BHJ) PSCs, revealing a bright future for commercialization.[7,8] The dramatic increase in PCE is mainly ascribed to the development of high-performance conjugated polymers.[9-12] The copolymerization of electron-donating (D) and electron-accepting (A) units has been widely used to construct new donor polymers.[13-21] The properties of copolymers, such as light absorption ability, energy levels and charge carrier mobility *etc.* can be effectively tuned by using different D and A monomers.[22-27]

Recently, terpolymers comprising three different units in the polymeric backbones have intrigued much attention since they can show synergetic effects through incorporating a third component (D or A) into D-A copolymers to form D-A-A or D-D-A type terpolymers,[28-31] rendering broad absorption, deep energy levels, high mobility, good solubility and miscibility, *etc.*[32-37] Wang and coworkers have recently reported a series of alternating terpolymers featuring D-A-A type molecular structure with quinoxaline and isoindigo as electron-withdrawing units.[38-40] These terpolymers showed broader absorption range compared to their corresponding D-A1 and D-A2 parent copolymers. The extended light absorption resulted in more generated excitons which mainly contribute to high photocurrent, leading to a PCE of 7.0%.[40] In another case, Janssen and coworkers have reported a PDPP3T*alt*TPT terpolymer (D-D-A type) composed of terthiophene (D1 = 3T), thiophene-phenylene-thiophene (D2 = TPT) donor units and diketopyrrolopyrrole (DPP) acceptor unit, which appears refined energy levels and optical bandgap comparing with its parent copolymers and subsequently a higher PCE of 8.0% was achieved.[41] Moreover, the crystallinity of copolymers can be fine-tuned through optimizing the monomers' ratios in random terpolymers with enhanced performance in PSCs.[42] Therefore, the terpolymer structure provides promising opportunities for finely tailoring polymers with popular optical-electronic properties through selection of appropriate third component. However, very limited examples of high-performance terpolymers have been reported.

In this paper, we presented two novel terpolymers named PtDDA and PtDAA, in which bithiophene (BT) and 5,7-bis(2-ethylhexyl)-4H,8H-benzo[1,2-c:4,5-c']dithiophene-4,8-dione (T1) were chosen as the donor and acceptor units, respectively. To ensure the coplanarity of terpolymers, thieno[3,2-b]thiophene (TT) and thiazolo[5,4-d]thiazole (TTz) as a third component were introduced into the polymer backbone. The molecular structures of PtDDA and PtDAA are shown in Scheme 1. When incorporating the electron-rich TT unit, PtDDA terpolymer shows a typical D1-D2-D1-A1 structure with two electron-rich building blocks and one electron-deficient building block. However, PtDAA shows a D1-A1-D1-A2 structure where TTz fused unit acts as an electron-deficient

---

[a] *School of Chemistry and Environment, Beihang University, Beijing 100191, P. R. China. E-mail: sunxb@buaa.edu.cn; huolijun@buaa.edu.cn; sunym@buaa.edu.cn.*
[b] *Heeger Beijing Research and Development Center, Beihang University, Beijing 100191, P. R. China.*
[c] *State Key Laboratory for Mechanical Behavior of Materials, Xi'an Jiaotong University, Xi'an 710049, P. R. China. E-mail: msewma@mail.xjtu.edu.cn.*

†Electronic Supplementary Information (ESI) available: [The experimental and characterization details of terpolymers, optimization of devices, AFM top morphology of active layers]. See DOI: 10.1039/x0xx00000x

View Article Online
DOI: 10.1039/C6TA05896H

building block because of the electron-withdrawing property of unsaturated nitrogen atom. The optical-electronic properties of two terpolymers were systematically investigated. Compared to PtDDA, PTDAA exhibits predominant advantages, such as broader absorption range, deeper HOMO level, higher hole transport mobility and favorable face-on orientation in BHJ films, which are beneficial to obtain excellent photovoltaic performance. As a result, a promising PCE of 8.1% has been achieved for PtDAA-based PSCs without using any additives or post-solvent/thermal annealing processes, which is much high than its analog PtDDA-based devices (PCE = 3.4%). Our results indicate that PtDAA terpolymer is a promising material for high-performance organic solar cells. Moreover, it is found that the subtle changes in the polymeric backbone (e.g. the replacement of the carbon atom with a nitrogen atom) can dramatically influence the photovoltaic performance of the terpolymers.

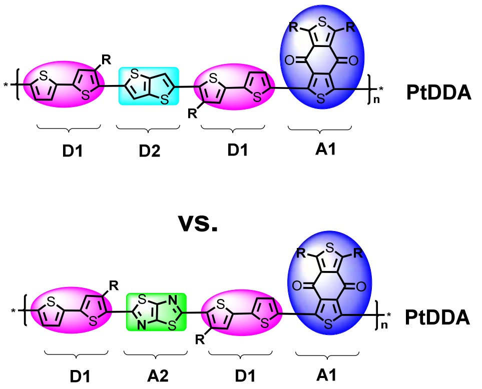

Scheme 1. Molecular structures of PtDDA (top) and PtDAA (down).

2 Experimental

The patterned ITO/glass substrates were ultrasonic cleaned successively in soapy water, deionized water, acetone and isopropanol. The cleaned ITO glasses were dried overnight in a vacuum oven at 110 ℃ and treated by UV-ozone for 20 min before using. PEDOT:PSS was spin casting onto the ITO glass at 4000 rpm for 40 s and annealed at 145 ℃ for 10 min in air. After that, PEDOT:PSS coated ITO/glass substrates were transferred into a glove box with nitrogen atmosphere. The mixture of PtDDA (orPtDAA):fullerene with different DIO contents (v/v) and D:A weight ratios was dissolved in 1,2-dichlorobenzene (DCB) with a total concentration of 30 mg/mL and stirred at 90 ℃ overnight. The blends were spin-cast onto PEDOT:PSS at 1600 rpm for 40 s to form the BHJ layers. Finally, Al (100 nm)/Ca (10 nm) layers were sequentially evaporated through a shadow mask. Current density-voltage (J–V) curves were measured using a Keithley 2400 Source Measure Unit. Solar cell performance used an Air Mass 1.5 Global (AM 1.5 G) solar simulator (Class AAA solar simulator, Model 94063A, Oriel) with an irradiation intensity of 100 mW•cm^{-2}, which was measured by a calibrated silicon solar cell and a readout meter (Model 91150V, Newport). IPCE spectra were measured by using a QEX10 Solar Cell IPCE measurement system (PV measurements, Inc.).

OFETs were fabricated in a bottom-gate/bottom-contact configuration in which the heavily n$^+$-doped Si layer acted as the gate electrode and the silicon oxide (SiO_2) was used as the dielectric layer. Gold source/drain electrodes with titanium as the adhesion layer were evaporated onto the SiO_2 layer. PtDDA and PtDAA were spin-coated onto OTS-treated SiO_2/Si substrates from chloroform solutions (2.5 mg mL^{-1}) at a spin-coating rate of 2500 rpm. The films were annealed at 160 °C for 5 min to get high mobility. The OFET performance was measured by using a Keithley 4200 semiconductor characterization system. The channel length (L) and width (W) are 20 μm and 1400 μm, respectively.

UV-vis absorption measurements were carried out on UV–vis spectrophotometer (Shimadzu, UV-3600). Atomic force microscopy (AFM) images were obtained using a NanoMan VS microscope in a tapping mode.

Hole-only devices were fabricated with a diode configuration of ITO/MoO_x/(PtDDA or PtDAA)/MoO_x/Al. The applied voltage is in the range of 0-6 V and the mobility was calculated by fitting the curves according to the equation: $J = 9\varepsilon_0\varepsilon_r\mu_h V^2/8L^3$, where J is the current density, ε_0 is the permittivity of free space, ε_r is the relative dielectric constant of the transport medium, μ_h is the hole mobility, V is the applied voltage, L is the film thickness.

The GIWAXS measurements were acquired at beamline 7.3.3 at Advanced Light Source[43]. Samples were prepared on Si substrate, and the 10 keV X-ray beam was incident at a grazing angle of 0.11°-0.15°，which maximized the scattering intensity from the samples. The data were analyzed by the Nika software package. The RSoXS transmission measurements were acquired at beamline 11.0.1.2 at Advanced Light Source[44]. Samples for RSoXS measurements were prepared on a PSS modified Si substrate under the same conditions as those used for device fabrication, and then transferred by floating in water to a 1.5 mm × 1.5 mm, 100 nm thick Si_3N_4 membrane supported by a 5 mm × 5 mm, 200 μm thick Si frame. The beam size at the sample is approximately 100 μm by 200 μm. Integrated scattering intensity profiles represent total scattered intensity at a given q. This was accomplished by averaging the data along the azimuth captured by the CCD and subsequently scaling the profiles by q^2. Scattering from the sample was captured by the CCD as far from the sample as possible (~150 mm) and with the CCD as close as possible (~50 mm). The profiles acquired from the two datasets were stitched together for an extended q-range.

3 Results and discussion

The synthetic routes of PtDDA and PtDAA are illustrated in Scheme 2. PtDDA and PtDAA were synthesized through the typical Stille-coupling polymerization in toluene, with $Pd(PPh_3)_4$ as the catalyst. To better understand the electronic distribution and backbone conformation of these two terpolymers, density functional theory (DFT) calculations at the B3LYP/6–31G (d,p) level of theory were performed. As shown in Figure S1 and S2, the highest occupied molecular orbital (HOMO) is delocalized along the entire polymer chain for both PtDDA and PtDAA. The lowest unoccupied molecular orbital (LUMO) surface is more localized on the T1 and TTz. The computational results confirm the electron-withdrawing properties of T1 and TTz. Meanwhile, the optimized molecular geometry of

View Article Online
DOI: 10.1039/C6TA05886H

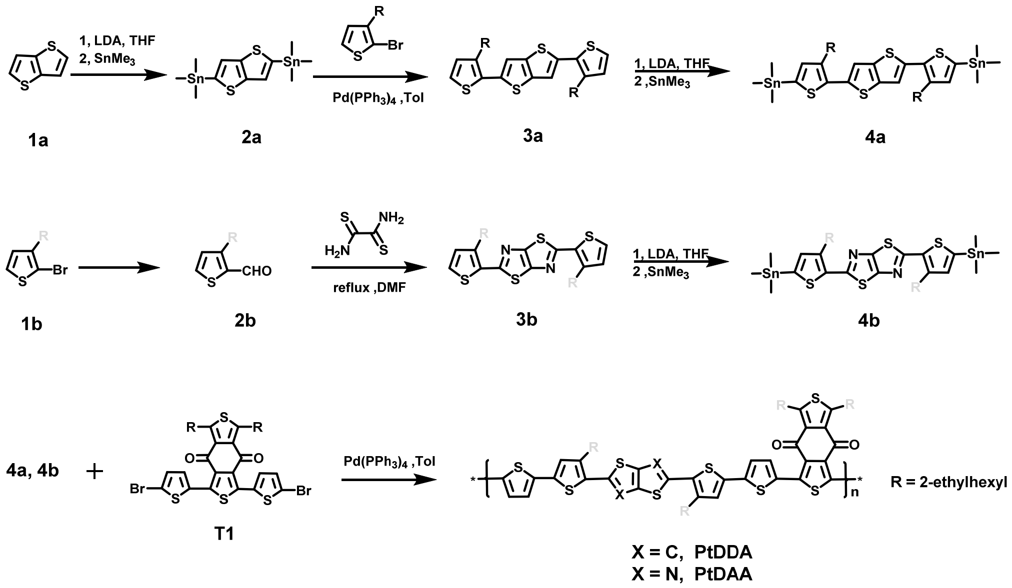

Scheme 2. Synthetic routes of PtDDA and PtDAA.

PtDAA trimers at the lowest energy exhibits a better planar structure than that of PtDDA (Figure S3). In addition, the electrostatic potential (ESP) maps of PtDDA and PtDAA are partly different (Figure S4), which is caused by the different electronegativity of carbon and nitrogen atoms between fused-ring TT and TTz, respectively.

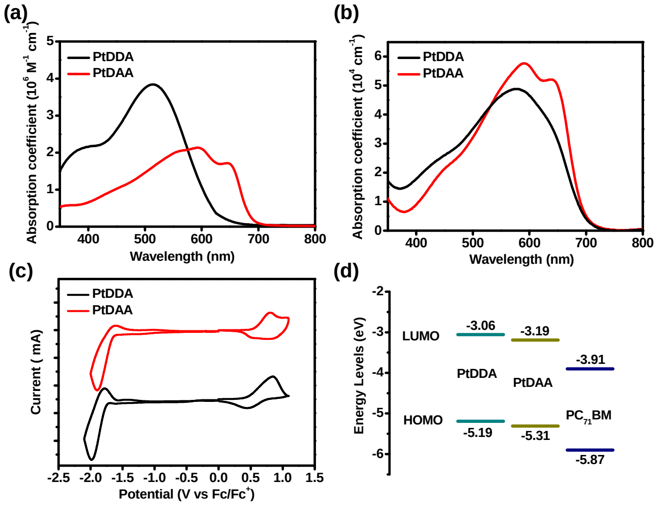

Figure 1. UV-vis absorption spectra of PtDDA and PtDAA in chloroform solution (a) and thin films (b); (c) Cyclic voltammogram curves of PtDDA and PtDAA; (d) Energy level diagrams of active layer components studied in the fabrication of devices.

The UV–vis absorption spectra of PtDDA and PtDAA were shown in Figure 1. The main absorption peak of PtDDA is located at 510 nm in a diluted chloroform solution and appears a pronounced red-shifted absorption by 77 nm to 587 nm in the solid state (Figure 1a). Meanwhile, the shoulder peak in PtDDA thin film located at ca. 650 nm implies a weak aggregation in PtDDA thin film. By contrast, the absorption spectra of PtDAA in solution and thin film appear similar profiles and the maximum absorption peaks are almost overlapped (~590 nm). Enhanced shoulder peak intensity was seen for the PtDAA thin film compared to its solution, which originates from the further strengthened intermolecular π-π aggregations. The results indicate PtDAA has stronger aggregated configurations than PtDDA even in a diluted solution. Thus it is primarily concluded that, as the third component inserted into D-A copolymer to form terpolymer, electronic-deficient TTz unit can induce stronger aggregation than TT unit. The maximum absorption coefficients of PtDAA ($\varepsilon = 5.8 \times 10^4$ cm^{-1}) is larger than that of PtDDA (4.9×10^4 cm^{-1}), indicating its better light-harvesting capability. The optical band gaps are calculated to be the similar values of 1.79 and 1.78 eV for PtDDA and PtDAA, respectively, from the onset of absorption spectra in the solid state.

Electrochemical cyclic voltammetry (CV) measurements were performed to characterize the energy levels of the two terpolymers (Figure 1c). The HOMO and LUMO levels were calculated from the onset of oxidation and reduction potentials using equations HOMO $= -(E_{ox} + 4.8)$ eV and LUMO $= -(E_{red} + 4.8)$ eV. As shown in Figure 1d, PtDDA exhibits a HOMO level of -5.19 eV, which is slightly higher than that of PtDAA (-5.31 eV). Considering that the open circuit voltage (V_{oc}) of PSCs is closely related to the offset between the HOMO level of donor and the LUMO level of acceptor, a deeper HOMO level of PtDAA will lead to a higher V_{oc}. The LUMO level of PtDDA is higher than PtDAA as well, with an offset value of 0.13 eV. The downshifted HOMO/LUMO levels of PtDAA may be caused by high electronegativity of unsaturated nitrogen atoms in TTz unit.

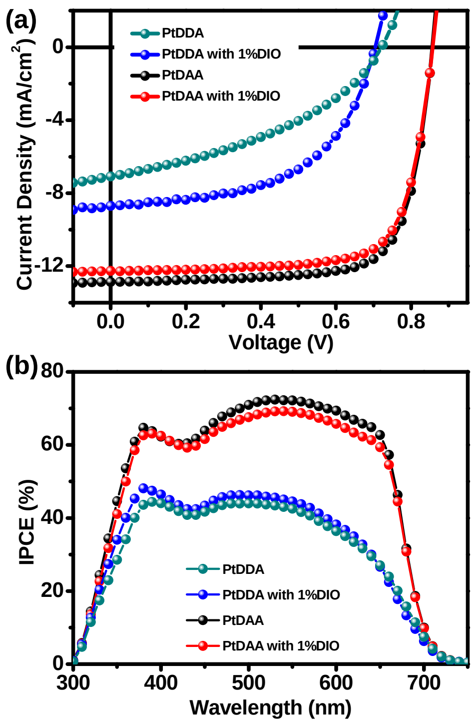

Figure 2. (a) *J-V* and (b) IPCE curves of PSCs based on PtDDA and PtDAA with $PC_{71}BM$ (1:1, w/w).

To further investigate the photovoltaic properties of PtDDA and PtDAA, organic solar cells were fabricated with a conventional configuration of ITO/PEDOT:PSS /terpolymers:$PC_{71}BM$/Ca/Al. The current density–voltage (*J–V*) characteristics of solar cells were measured under AM 1.5 G illumination with an intensity of 100 mW/cm^2. The blend films with different additive (1,8-diiodooctane, DIO) concentrations and donor/acceptor weight ratios were processed to optimize the device performance. It was found that the use of DIO could improve the efficiency of PtDDA-based solar cells. In contrast, there is no effect for PtDAA-based devices. Without using DIO, the solar cells showed better PCEs (Figure S5, S6). The optimized weight ratio was found to be at 1:1 for PtDDA and PtDAA-based devices (Figure S5, S6). Figure 2a showed the *J-V* curves of the champion cells and the device parameters are summarized in Table 1. For PtDDA PSCs processed without DIO, the V_{oc}, J_{sc} and FF is 0.72 V, 7.18 mA/cm^2 and 0.40, respectively, resulting in a low PCE of 2.0%. When processed with 1% DIO, the PCE was increased up to 3.4%, mainly due to the increased J_{sc} (8.69 mA/cm^2) and FF (0.55%). For as cast BHJ films without using any additive, PtDAA:$PC_{71}BM$ solar cells achieve a high V_{oc} of 0.86 V, a J_{sc} of 12.87 mA/cm^2 and a high FF of 0.74, with an overall PCE of 8.1%. To the best of our knowledge, the PCE of 8.1% represents one of the highest values so far for the PSCs based on terpolymers (see Table 2). Additionally, an average PCE of 8.0% within a small standard deviation of 0.1% was obtained, revealing the good reproducibility of high performance for PtDAA-based solar cells. Meanwhile, the addition of DIO could not further increase the cell efficiency. When processed with 1% DIO, PtDAA:$PC_{71}BM$ device exhibits a decreased PCE of 7.7%, with a V_{oc} of 0.86 V, a J_{sc} of 12.25 mA/cm^2 and a FF of 0.74. The relatively higher V_{oc} achieved in PtDAA-based solar cells is consistent with the deeper HOMO level of PtDAA than that of PtDDA.

To verify the J_{sc} difference between PtDAA- and PtDDA-based devices, the incident photon conversion efficiency (IPCE) spectra were measured to make the direct comparison (Figure 2b). For PtDDA-based solar cells, the addition of DIO slightly increased the IPCE values. However, the maximum IPCE value is about 40%. Incontrast, higher IPCE values over 60% were observed in the wavelength range of 370-650 nm for PtDAA-based devices. Especially, the maximum value of 72.5% was found around 490 nm for as-cast PtDAA solar cells, indicating the efficient photon generation and charge collection within the device. The integrated J_{sc} of PTDAA solar cells obtained from IPCE curve is 12.72 mA/cm^2, which agrees well with the value of 12.87 mA/cm^2 measured under the simulated light with a mismatch less than 2%.

Charge carrier transport properties of PtDDA and PtDAA films were studied using organic field-effect transistors (OFETs). Typical output and transfer curves are presented in Figure 3. As can be seen from the transfer curves, the devices show typical p-type transport properties. PtDAA shows a high mobility of 0.28 cm^2 V^{-1} s^{-1}, which is approximately one order of magnitude of higher than that of PtDDA (0.035 cm^2 V^{-1} s^{-1}). The significant difference in carrier mobility strongly related to the molecular crystallinity and orientation, which will be discussed in the following analysis. The mobility was also measured using space charge limited current (SCLC) method (Figure S7) and the values are 0.77×10^{-3} and 3.44×10^{-3} cm^2 V^{-1} s^{-1} for PtDDA and PtDAA, respectively, agreeing well with OFETs results.

It is well-known that photovoltaic properties are affected by the active layer morphology. In order to gain insight into the morphology of these terpolymer:$PC_{71}BM$ blends, atomic force microscopy (AFM) measurements were carried out. As shown in Figure S8, PtDDA:$PC_{71}BM$ blend films show smoother surface with a root-mean-square (RMS) roughness of 0.45 nm. However, the surface of PtDAA:$PC_{71}BM$ blend film exhibits lager domain size and apparent rough surface morphology, with RMS value of 1.21 nm. The addition of DIO increased the surface roughness of both terpolymer: $PC_{71}BM$ blend films.

The molecular orientation and packing in neat and blended films were investigated by grazing incidence wide angle X-ray scattering (GIWAXS) measurements. The two-dimensional (2D) GIWAXS patterns for neat and blend films of PtDDA and PtDAA, with the corresponding out-of-plane and in-plane scattering profiles are shown in Figure 4. The reflection peaks located at q ≈ 0.30 Å^{-1} for PtDAA and PtDDA neat films in the in-plane direction are coming from the (100) lamellar packing of the terpolymers. The lamellar (100) peak and π-π stacking (010) peak in the out-of-plane direction

View Article Online
DOI: 10.1039/C6TA05886H

Table 1. Device performance of solar cells based on PtDDA and PtDAA with $PC_{71}BM$ (1:1, w/w) in a conventional device architecture.

Material	DIO [%]	V_{oc} [V]	J_{sc} [mA/cm^2]	FF	PCE^a [%]	PCE^{max} [%]
PtDDA	0	0.715±0.005	7.02±0.12	0.40±0.02	2.0±0.1	2.1
	1	0.706±0.001	8.29±0.22	0.54±0.01	3.2±0.1	3.4
PtDAA	0	0.859±0.003	12.87±0.18	0.73±0.01	8.0±0.1	8.1
	1	0.859±0.003	11.83±0.30	0.74±0.01	7.5±0.2	7.7

[a] The average values are obtained from 6 devices.

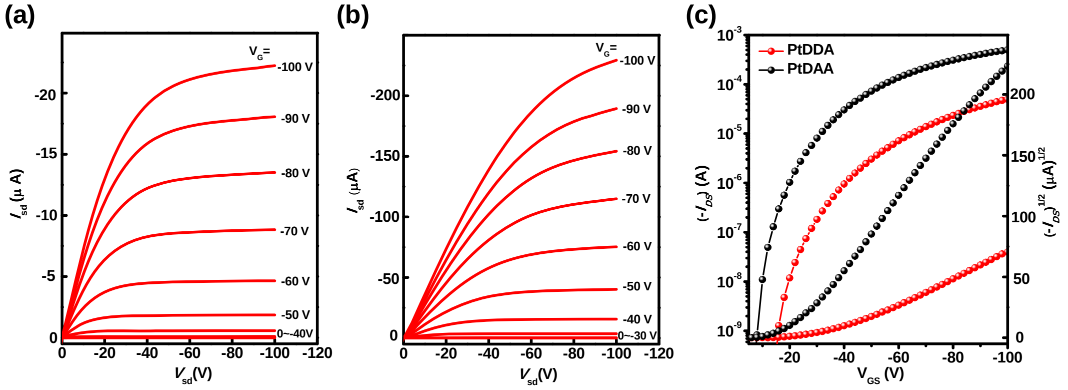

Figure 3. Output curves of OFETs based on a) PtDDA and b) PtDAA after thermal annealing at 160°C. c) Corresponding transfer characteristics of PtDDA (red) and PtDAA (black).

for neat PtDDA film are located at q ≈ 0.35 and 1.72 Å^{-1}, with d-spacing of approximately 1.79 nm and 0.37 nm, respectively. In the in-plane direction, the (010) diffraction peak of PtDDA is nonexistent, indicating a preference for the face-on molecular orientation in neat PtDDA film. For PtDAA neat film, a stronger edge-on and weak face-on orientation of (010) π-π stacking peaks are observed, and located at q ≈ 1.78 Å^{-1}, with corresponding packing space of 0.35 nm. Thus, the edge-on and face-on polymer backbone orientation are coexisting in PtDAA film. However, compared to PtDDA, PtDAA showed shorter π–π stacking distance, indicating better crystallinity, which agrees well with the SCLC results.

When blended with $PC_{71}BM$, two blend films show obvious and broad diffraction halo at q ≈ 1.32 Å^{-1}, which are attributed to the aggregation of $PC_{71}BM$. As for PtDDA blend film, either the in-plane or out-of-plane profile shows no obvious reflection peak. The absence of π–π stacking reflection in PtDDA:$PC_{71}BM$ blend film indicates that the face-on molecular orientation of PtDDA neat film is disrupted by the $PC_{71}BM$. For PtDAA:$PC_{71}BM$ film, compared to its neat film, the (010) reflection peak located at 1.77 Å^{-1} is enhanced in the out-of-plane direction and decreased in the in-plane direction, indicating a more face-on orientation of PtDAA polymer in the blend. The face-on crystallites were considered to be beneficial for charge carrier transport. When processed with additive DIO, the (100) peak of PtDDA in the out-of-plane direction is stronger, indicating the lamellar packing of PtDDA is significantly increased, which explains why the device performance is greatly enhanced after processed with additive. In contrast, the PtDAA blends show similar diffraction profiles with slightly enhanced π–π stacking in the in-plane and out-of-plane directions, which is in agreement with the trend of the device performance.

Table 2. Comparison of optical bandgap, energy levels and photovoltaic characteristics of reported terpolymers with different alternating structures.

Donor	Alternating structure	Acceptor	E_g^{opt} (eV)	HOMO/LUMO^a (eV)/(eV)	V_{oc} (V)	J_{sc} (mA cm^{-2})	FF (%)	PCE (%)	Ref.
PtDDA	D1-D2-D1-A	$PC_{71}BM$	1.79	-5.19/-3.06	0.70	8.69	0.55	3.4	This work
PtDAA	D-A1-D-A2	$PC_{71}BM$	1.78	-5.31/-3.19	0.86	12.87	0.74	8.1	This work
PDPP2T-DTP	D-A1-D-A2	$PC_{71}BM$	1.23	-5.26/-3.68	0.43	16.6	0.54	3.9	28
Reg-PBDPPT	D1-A-D2-A	$PC_{71}BM$	1.42	−5.25/−3.83	0.62	12.29	0.71	5.5	29
Ran-PBDPPT	Random	$PC_{71}BM$	1.41	−5.29/−3.88	0.61	13.18	0.65	5.2	29
BDTA-PTQD	D-A1-D-A2	$PC_{71}BM$	1.50	-5.44/-3.84	0.84	11.74	0.63	6.2	30

PDTSTTBDT[b]	D1-A-D2-A	$PC_{71}BM$	1.45	−5.19/−3.62	0.62	14.77	0.61	6.1	31
BFS4[b]	D1-A-D2-A	$PC_{61}BM$	1.56	- / -	0.90	14.20	0.61	7.8	32
PBDT-O-ADA[b]	D1-A-D2-A	$PC_{71}BM$	1.61	-5.29/-3.63	0.74	12.20	0.46	4.1	37
P3TQTI-F	D-A1-D-A2	$PC_{71}BM$	1.56	-5.47/-3.93	0.67	15.5	0.67	7.0	40
PDPP3TaltTPT	D1-A-D2-A	$PC_{71}BM$	1.43	- /-3.73	0.75	15.9	0.67	8.0	41
P2[b]	Random	$PC_{71}BM$	1.33	−5.22/−3.53	0.67	16.22	0.66	7.2	42

[a] Measured by the cyclic voltammetry. [b] Achieved with an inverted architecture.

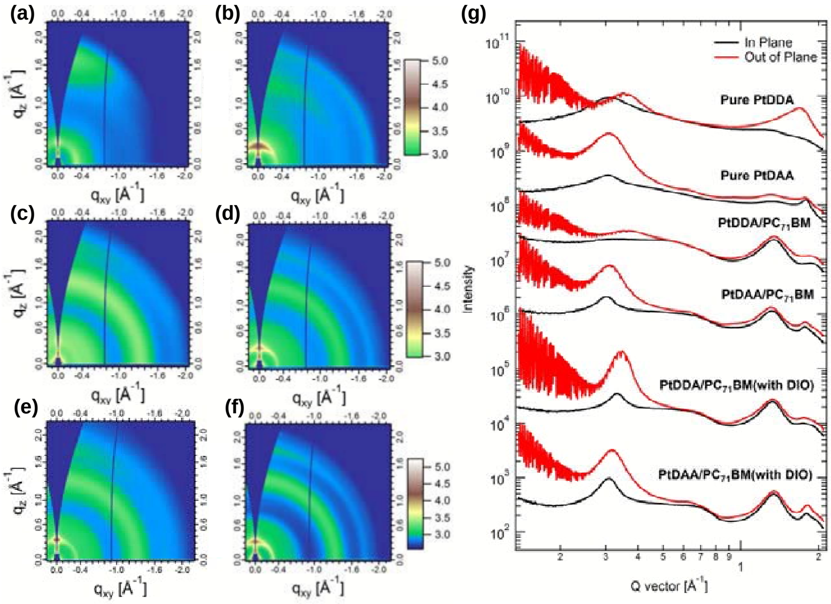

Figure 4. GIWAXS patterns of neat films and blends with $PC_{71}BM$. 2D GIWAXS patterns of a) PtDDA neat film, b) PtDAA neat film, c) PtDDA:$PC_{71}BM$ blend film and d) PtDAA: $PC_{71}BM$ blend film (1% DIO), e) PtDAA:$PC_{71}BM$ blend film and f) PtDAA:$PC_{71}BM$ blend film (1% DIO). g) Line curves in out-of-plane and in-plane direction from 2D GIWAXS patterns.

Furthermore, resonant soft X-ray scattering (R-SoXS) was used to study the feature of phase separation in their respective blend films (Figure 5). The resonant energy of 284.2 eV was selected to provide optimized scattering contrast.[44] As cast PtDAA:$PC_{71}BM$ blend shows an interference at q ~ 0.16 nm^{-1}, corresponding to a mode domain spacing (centre-to-centre) of ~39 nm, which is larger than that of ~17 nm for PtDDA:$PC_{71}BM$ blend film. When DIO additive was used, domain spacing of PtDAA:$PC_{71}BM$ and PtDDA:$PC_{71}BM$ films are increased up to 45 nm and 70 nm, respectively. This is consistent with the results observed from the AFM morphology. In addition, it is noted that average composition variations of BHJ blends can be estimated through integrating R-SoXS scattering profiles.[45,46] As shown in Figure 5, the total scattering intensity (TSI) for as cast PtDAA:$PC_{71}BM$ film is slightly lower than that of blend processed with 1% DIO, latter. This is consistent with the slight fluctuation of FF. Furthermore, the scattering profiles of PtDDA based blend changes dramatically after the addition of 1% DIO. The total scattering intensity of PtDDA:$PC_{71}BM$ with 1% DIO is much higher than that without additive, revealing that the addition of DIO leads to higher average domain purity and result in the significant increases in the FF. Generally, high average domain purity is beneficial to restrain charge carrier recombination and finally enhance the device performance. Thus, DIO improved performance of PtDDA based solar cells mainly attributes to the increase of the relative purity. However, PtDAA:$PC_{71}BM$ is less influenced by DIO. Higher average domain purity results in enhanced FF but not the overall device performance.

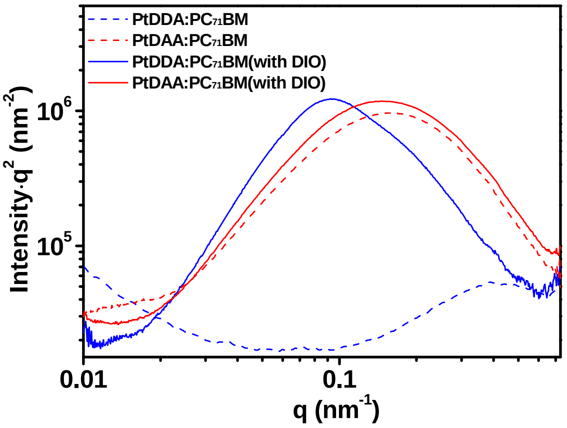

Figure 5. Resonant soft x-ray scattering in log scale for PtDDA:$PC_{71}BM$ and PtDAA:$PC_{71}BM$ blended films with and without 1% DIO.

4. Conclusions

In conclusion, two novel terpolymers named PtDDA and PtDAA were synthesized and characterized. The incorporation of TT and TTz units afforded two different backbone alternating structures of D1-D2-D1-A1 (D-D-A type) for PtDDA and D1-A1-D1-A2 (D-A-A type) for PtDAA. Due to the higher electronegativity of nitrogen atoms in TTz fused rings, PtDAA exhibits better ordered molecular structure, stronger aggregation tendency and deeper HOMO level compared to PtDDA. Solar cells based on PtDAA showed a high PCE of 8.1%, with a V_{oc} of 0.86 V, a J_{sc} of 12.87 mA/cm^2 and FF of 0.74. The high efficiency of 8.1% is one of the highest values so far for the PSCs based on conjugated terpolymers, which mainly originates from the efficient carrier transport in the active layer, high crystallinity of the terpolymer, and high domain purity. This work shows that D-A-A type terpolymer is a promissing candidate for the fabrication of high performance solar cells.

Acknowledgements

B.F. and X.X. contributed equally to this work. This work was financially supported by the National Natural Science Foundation of China (NSFC) (nos. 51473009, 51273203, 51261160496, 21504006, 21534003), the International Science & Technology Cooperation Program of China (no. 2014DFA52820) and the 111 project (B14009). The authors thank Prof. Donghui Wei and Prof. Mingming Yu (Zhengzhou University) for assistance in performing Gaussian DFT calculations. Y.S. gratefully acknowledges Prof. Zhaohui Wang (ICCAS) for the assistance with OFETs measurements. The X-ray data was acquired at beamline 7.3.3 and 11.0.1.2 at the Advanced Light Source, which is supported by the Director, Office of Science, Office of Basic Energy Sciences, of the U.S. Department of Energy under Contract No. DE-AC02-05CH11231.

Notes and references

1 J. J. M. Halls, C. A. Walsh, N. C. Greenham, E. A. Marseglia, R. H. Friend, S. C. Moratti and A. B. Holmes, *Nature,* 1995, **376**, 498–500.
2 S. H. Park, A. Roy, S. Beaupre, S. Cho, N. Coates, J. S. Moon, D. Moses, M. Leclerc, K. Lee and A. J. Heeger, *Nat. Photon.,* 2009, **3,** 297-303.
3 R. Søndergaard, M. Hösel, D. Angmo, T. T. Larsen-Olsen and F. C. Krebs, *Mater. Today,* 2012, **15,** 36-49.
4 Y. Liu, J. Zhao, Z. Li, C. Mu, W. Ma, H. Hu, K. Jiang, H. Lin, H. Ade and H. Yan, *Nat. Commun.,* 2014, **5,** 5293.
5 L. Lu, T. Xu, W. Chen, E. S. Landry and L. Yu, *Nat. Photon.,* 2014, **8,** 716-722.
6 S. Nam, J. Seo, S. Woo, W. H. Kim, H. Kim, D. D. Bradley and Y. Kim, *Nat. Commun.,* 2015, **6,** 8929.
7 G. Yu, J. Gao, J. C. Hummelen, F. Wudl and A. J. Heeger, *Science,* 1995, **270,** 1789-1791.
8 J. Zhao, Y. Li, G. Yang, K. Jiang, H. Lin, H. Ade, W. Ma and H. Yan, *Nat. Energy,* 2016, **1,** 15027.
9 Y.-J. Cheng, S.-H. Yang and C.-S. Hsu, *Chem. Rev.,* 2009, **109,** 5868-5923.
10 Y. Li, *Acc. Chem. Res.,* 2012, *45*, 723-733.
11 L. Lu, T. Zheng, Q. Wu, A. M. Schneider, D. Zhao and L. Yu, *Chem. Rev.,* 2015, **115,** 12666-12731.
12 W. Yue, R. S. Ashraf, C. B. Nielsen, E. Collado-Fregoso, M. R. Niazi, S. A. Yousaf, M. Kirkus, H. Y. Chen, A. Amassian, J. R. Durrant and I. McCulloch, *Adv.Mater.,* 2015, **27,** 4702-4707.
13 M. Svensson, F. Zhang, S. C. Veenstra, W. J. H. Verhees, J. C. Hummelen, J. M. Kroon, O. Inganäs and M. R. Andersson, *Adv.Mater.,* 2003, **15,** 988-991.
14 J. Peet, J. Y. Kim, N. E. Coates, W. L. Ma, D. Moses, A. J. Heeger and G. C. Bazan, *Nat. Mater.,* 2007, **6,** 497-500.
15 J. Hou, H.-Y. Chen, S. Zhang, G. Li and Y. Yang, *J. Am. Chem. Soc.,* 2008, **130,** 16144-16145.
16 H. Zhou, L. Yang, A. C. Stuart, S. C. Price, S. Liu and W. You, *Angew. Chem. Int. Ed.,* 2011, **50,** 2995-2998.
17 L. Huo, T. Liu, B. Fan, Z. Zhao, X. Sun, D. Wei, M. Yu, Y. Liu and Y. Sun, *Adv.Mater.,* 2015, **27,** 6969-6975.
18 L. Huo, T. Liu, X. Sun, Y. Cai, A. J. Heeger and Y. Sun, *Adv.Mater.,* 2015, **27,** 2938-2944.
19 A. Najari, S. Beaupré, N. Allard, M. Ouattara, J.-R. Pouliot, P. Charest, S. Besner, M. Simoneau and M. Leclerc, *Adv. Energy Mater.,* 2015, **5,** 1501213.
20 S. Nishinaga, H. Mori and Y. Nishihara, *Macromolecules,* 2015, **48,** 2875-2885.
21 S. Liu, X. Bao, W. Li, K. Wu, G. Xie, R. Yang and C. Yang, *Macromolecules*, 2015, **48**, 2948−2957.
22 S. Subramaniyan, F. S. Kim, G. Ren, H. Li and S. A. Jenekhe, *Macromolecules,* 2012, **45,** 9029-9037.
23 J. D. Yuen, J. Fan, J. Seifter, B. Lim, R. Hufschmid, A. J. Heeger and F. Wudl, *J. Am. Chem. Soc.,* 2011, **133,** 20799-20807.
24 H. Hu, K. Jiang, G. Yang, J. Liu, Z. Li, H. Lin, Y. Liu, J. Zhao, J. Zhang, F. Huang, Y. Qu, W. Ma and H. Yan, *J. Am. Chem. Soc.,* 2015, **137,** 14149-14157.
25 B. Xia, K. Lu, L. Yuan, J. Zhang, L. Zhu, X. Zhu, D. Deng, H. Li and Z. Wei, *Polym. Chem.,* 2016, **7,** 1323-1329.
26 M. Zhang, X. Guo, W. Ma, H. Ade and J. Hou, *Adv.Mater.,* 2015, **27,** 4655-4660.
27 J. Zhao, Y. Li, A. Hunt, J. Zhang, H. Yao, Z. Li, J. Zhang, F. Huang, H. Ade and H. Yan, *Adv.Mater.,* 2015, **28,** 1868-1873.
28 W. Li, K. H. Hendriks, A. Furlan, A. Zhang, M. M. Wienk and R. A. Janssen, *Chem. Commun.,* 2015, **51,** 4290-4293.
29 E. Y. Ko, G. E. Park, D. H. Lee, H. A. Um, J. Shin, M. J. Cho and D. H. Choi, *ACS Appl. Mater. Interfaces,* 2015, **7,** 28303-28310.
30 H. Heo, H. Kim, D. Lee, S. Jang, L. Ban, B. Lim, J. Lee and Y. Lee, *Macromolecules,* 2016, **49,** 3328-3335.
31 M. L. Keshtov, S. A. Kuklin, D. Y. Godovsky, A. R. Khokhlov, R. Kurchania, F. C. Chen, E. N. Koukaras and G. D. Sharma, *J. Polym. Sci., Part A: Polym. Chem.,* 2016, **54,** 155-168.
32 T. Qin, W. Zajaczkowski, W. Pisula, M. Baumgarten, M. Chen, M. Gao, G. Wilson, C. D. Easton, K. Mullen and S. E. Watkins, *J. Am. Chem. Soc.,* 2014, **136,** 6049-6055.
33 T. E. Kang, K.-H. Kim and B. J. Kim, *J. Mater. Chem. A,* 2014, **2,** 15252-15267.
34 Q. Fan, Y. Liu, M. Xiao, W. Su, H. Gao, J. Chen, H. Tan, Y. Wang, R. Yang and W. Zhu, *J. Mater. Chem. C,* 2015, **3,** 6240-6248.
35 S. Hedstrom, Q. Tao, E. Wang and P. Persson, *Phys. Chem. Chem. Phys.,* 2015, **17,** 26677-26689.
36 K. H. Hendriks, G. H. L. Heintges, M. M. Wienk and R. A. J. Janssen, *J. Mater. Chem. A,* 2014, **2,** 17899-17905.
37 X. Huang, G. Zhang, C. Zhou, L. Liu, Y. Jin, S. Liu, L. Ying, F. Huang and Y. Cao, *Polym. Chem.,* 2015, **6,** 4154-4161.
38 D. Dang, W. Chen, R. Yang, W. Zhu, W. Mammo and E. Wang, *Chem. Commun.,* 2013, **49,** 9335-9337.
39 W. Sun, Z. Ma, D. Dang, W. Zhu, M. R. Andersson, F. Zhang and E. Wang, *J. Mater. Chem. A,* 2013, **1,** 11141.
40 Q. Tao, Y. Xia, X. Xu, S. Hedström, O. Bäcke, D. I. James, P. Persson, E. Olsson, O. Inganäs, L. Hou, W. Zhu and E. Wang, *Macromolecules,* 2015, **48,** 1009-1016.
41 K. H. Hendriks, G. H. Heintges, V. S. Gevaerts, M. M. Wienk and R. A. Janssen, *Angew. Chem. Int. Ed.,* 2013, **52,** 8341-8344.

View Article Online
DOI: 10.1039/C6TA05886H

42 K.-H. Kim, S. Park, H. Yu, H. Kang, I. Song, J. H. Oh and B. J. Kim, *Chem. Mater.,* 2014, **26,** 6963-6970.

43 E. Gann, A. T. Young, B. A. Collins, H. Yan, J. Nasiatka, H. A. Padmore, H. Ade, A. Hexemer and C. Wang, *Rev. Sci. Instrum.,* 2012, **83,** 045110.

44 A. Hexemer, W. Bras, J. Glossinger, E. Schaible, E. Gann, R. Kir ian, A. MacDowell, M. Church, B. Rude, H. Padmore, *J. Phys. Conf. Ser.,* 2010, **247,** 012007.

45 J. R. Tumbleston, B. A. Collins, L. Yang, A. C. Stuart, E. Gann, W. Ma, W. You and H. Ade, *Nat. Photon.,* 2014, **8,** 385-391.

46 Y. Lin, F. Zhao, Q. He, L. Huo, Y. Wu, T. C. Parker, W. Ma, Y. Sun, C. Wang, D. Zhu, A. J. Heeger, S. R. Marder and X. Zhan, *J. Am. Chem. Soc.,* 2016, **138,** 4955-4961.

View Article Online
DOI: 10.1039/C6TA05886H

ToC figure